Scientific Research

Experimental Study on the Bonding Behavior between Ribbed Steel Bars and Ultra-High-Performance Concrete

Xinzhi Duan [1,2,3]

[1] Shanghai Municipal Planning & Design Institute Co., Ltd., Shanghai 200031, China;
[2] Shanghai Chentou Urban Development Institute Co.,Ltd., Shanghai 200031,China;
[3] Shanghai Engineering Research Center of Urban Road Ecological Technology, Shanghai 201418, China.
Correspondence: 496024331@qq.com

Abstract: To evaluate the bonding behavior between ribbed steel bars and ultra-high-performance concrete (UHPC), several pull-out samples were experimentally investigated and presented. The influences of bar diameter and embedment length on the bond failure mode, ultimate bond stress, stress–slip curve and bond stress distribution were investigated. Compared with that of ordinary reinforced concrete, the ultimate bond stress between steel bars and UHPC was increased by 74% under the same conditions. In addition, the bond-slip curve showed a relatively large slope before the ultimate bond stress was reached, and at the same time, the curve showed better ductility after the ultimate bond stress was exceeded. When the sample experiences steel bar yielding or pull-out failure, the bond stress distribution curve exhibits typical multipeak features. As the bar embedment length increased, the bond stress distribution became increasingly heterogeneous, and the increase in the peak number in the bond stress distribution curve reflected this trend. Under appropriate concrete cover thickness, the critical embedment length was between 4d and 6d.

Keywords: ultra-high-performance concrete; steel fiber; ribbed steel bar; bond stress; bond-slip curve

Citation: Duan, X. Experimental Study on the Bonding Behavior between Ribbed Steel Bars and Ultra-High-Performance Concrete. *Prestress Technology* **2025**, 3, 52-64. https://doi.org/10.59238/j.pt.2025.03.004

Received: 14/06/2025
Accepted: 15/08/2025
Published: 30/08/2025

Publisher's Note: Prestress technology stays neutral with regard to jurisdictional claims in published maps and institutional affiliations.

1 Introduction

Ultra-high-performance concrete (UHPC) is a new type of ultra-high-performance cement-based material. This material was first successfully developed by the French company BOUYGUES; initially, it was referred to as reactive powder concrete (RPC) [1]. Over the past decade, research on the preparation methods, microstructural characteristics, and basic mechanical properties of UHPC materials based on the RPC preparation principle has attracted widespread attention from scholars worldwide [2]. Compared with commonly used ordinary concrete, UHPC has outstanding advantages in terms of compressive strength, tensile strength, durability, and water resistance. UHPC is composed mainly of high-strength cement, silica fume, fine aggregate, steel fibers, and high-efficiency water-reducing agents. The preparation principle of UHPC involves optimizing the particle size distribution to form a densely packed matrix and adding steel fibers in a certain proportion to enhance the bridging effect between the UHPC matrix materials [3-5]. To date, many scholars in China and other countries have conducted preliminary research on the preparation and engineering application of UHPC and have reported valuable results [6-12]. Good bond between steel bars and concrete is the foundation for their collaborative work. The bond force primarily includes chemical adhesive force, mechanical interlocking force, and frictional force [13]. The high compressive strength and high elastic modulus of UHPC enhance the mechanical interlocking force between the matrix and steel bars. Moreover, steel fibers can suppress the initiation and development of cracks within UHPC, further improving the friction and mechanical interlocking forces between steel bars and UHPC [14-16]. Many factors affect the bond

https://doi.org/10.59238/j.pt.2025.03.004

performance between steel bars and ordinary concrete, including the diameter of the steel bars, the anchorage length, the thickness of the concrete cover layer, and the strength of the base material [17-27]. Currently, research on the bond performance between steel bars and ultra-high-performance concrete (UHPC) is limited. Owing to its dense microstructure and excellent comprehensive mechanical properties, UHPC exhibits bond performance characteristics that are distinct from those of ordinary concrete. Whether existing research findings on the bond performance between steel bars and ordinary concrete are applicable to the bond interface between steel bars and UHPC remains to be discussed. In this paper, the bond performance between ribbed steel bars and ultrahigh performance concrete (UHPC) is investigated through experimental studies, and the bond failure mechanisms and mechanical properties of the bond between steel bars and UHPC under the influence of multiple factors are explored. The findings provide technical guidance for the design of bonded anchorage between steel bars and UHPC in future new construction and reinforcement/repair projects.

2 Test Overview

The experimental design in this paper is based on the pull-out test scheme proposed by Yuan and Graybeal [28], which can be used to simulate the stress conditions of the bond interface at the anchorage location of steel bars in concrete materials in actual engineering. The main parameters studied in this experiment include the diameter of the steel bar and the bond length of the steel bar.

2.1 Test Materials

The mix proportion of the UHPC material used in this test is shown in Table 1. The main materials include P·O 52.5 cement, silica fume, river sand, water, copper-coated straight steel fibers (12 mm in length and 0.2 mm in diameter), and polycarboxylate superplasticizer. Axial compression and axial tension tests were conducted on the samples. The 28-day axial tensile strength ranged from 6.5 to 7.5 MPa, while the 28-day axial compressive strength was approximately 150 MPa. HRB335-grade ribbed steel bars with an average yield strain of about 2300 $\mu\varepsilon$ were used as the embedded reinforcement. The test setup for evaluating the axial compression and tensile properties of the UHPC material is illustrated in Figure 1.

Table 1 Material mix ratio (percentage by mass)

52.5 cement	Silica fume	River sand	Water	Water-reducing agent	Steel fiber
35.4	7.1	42.5	7.8	0.2	7.0

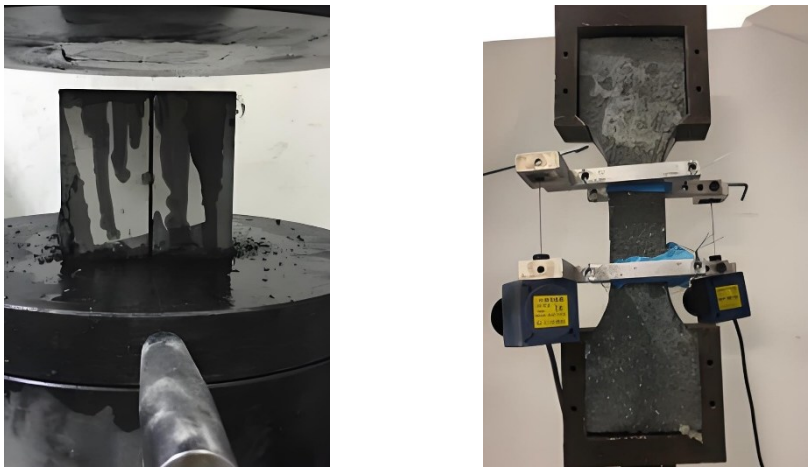

a) Axial compression test setup b) Axial tension test setup

Figure 1 Assembly of the UHPC material property test setup

2.2 Test Samples Design and Production

The samples in this study consisted of 8 center-pull samples. The samples were fabricated using steel bars of different diameters (18 mm, 22 mm, and 32 mm) and different embedded lengths (4d, 6d, and 8d) to investigate the effects of steel bar diameter and bond length on bond performance and the failure mode between steel bars and UHPC. The parameters of each sample are shown in Table 2, with a steel bar cover thickness of 3d for all the samples. When the samples were being made, a 300 mm thick UHPC layer was precast on the reinforced concrete cast-in-place base slab. The UHPC layer was anchored to the reinforced concrete base slab using embedded ribbed steel bars. The sample design is shown in Figure 2.

Table 2 Parameters of each pull-out sample

No. of sample	Diameter of steel bar /mm	Anchorage length/diameter (l_a/d)	Cover thickness
S1	18	4.0	3d
S2	22	4.0	3d
S3	32	4.0	3d
S4	18	4.0	3d
S5	18	6.0	3d
S6	18	8.0	3d
S7	18	6.0	3d
S8	22	6.0	3d
S9	32	6.0	3d

Note: The diameter of the steel bar was selected based on commonly used values in bridge engineering. The anchorage length was determined with reference to the research findings of [28], specifically to achieve two failure modes (pull-out failure and matrix failure) and to investigate the designed anchorage length of ribbed steel bar.

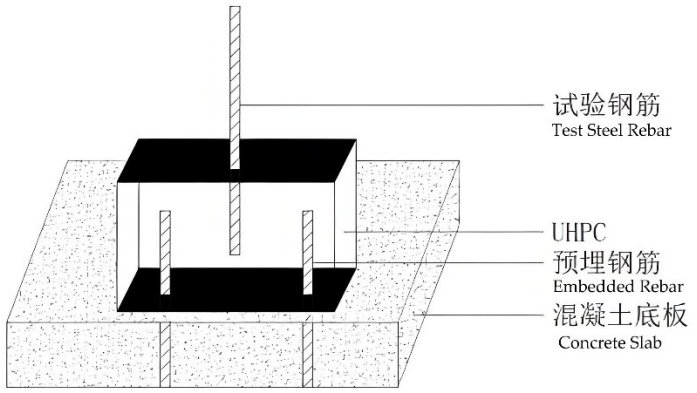

Figure 2 Pull-out test sample design

To obtain the strain distribution of the ribbed steel bar along the bonded segment during the central pull-out tests, strain gauges were internally installed after pre-milling grooves on the bar. The procedure involved first splitting the steel bar symmetrically along its central axis. Each half-bar was milled with a groove measuring 4 mm × 2 mm (width × depth). After reassembling the two halves, the combined groove formed a 4 mm × 4 mm cross-section. Strain gauges were uniformly distributed along the bonded segment of the specimen with a spacing of one steel bar diameter. The configuration of the strain gauges attached to the steel bar surface is shown in Figure 3 below.

 https://doi.org/10.59238/j.pt.2025.03.004

Figure 3 Strain gauges attached to the inside of the steel bars

2.3 Loading System and Test Methods

The test setup is shown in Figure 4 below. First, a hydraulic jack was positioned on a custom-designed steel frame, which was supported by a pre-cast reinforced concrete slab. The tensile and compressive strength as well as the deformation of the steel frame had been pre-verified through calculations. Steel bars of different diameters were equipped with matching clamps at the free end. The loading assembly is illustrated in Figure 5. The pull-out force was applied under force control throughout the test, with a loading rate of 100 N/s. The pulled steel bar remained in tension during the entire process. The test ended when either sample failure occurred or the load could no longer be increased.

Figure 4 Loading device

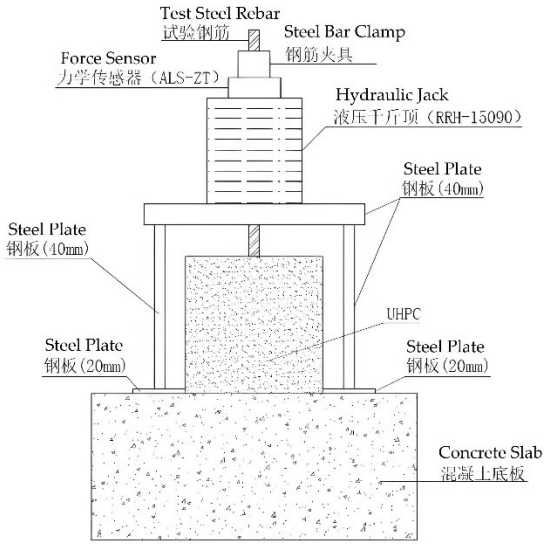

Figure 5 Experimental setup diagram

A force sensor between the jack and the steel bar clamp was used to monitor the pull-out force. Three displacement sensor holders fixed at 120° intervals were mounted at the end of the steel bar sample to measure the pull-out displacement, with the fixed bracket for the displacement sensors shown in Figure 6 below. Data from both the force sensor and displacement sensors were collected and recorded using a DH3818 data acquisition system.

Figure 6 Fixed bracket for displacement sensors

3 Analysis of Experimental Phenomena and Results

3.1 Failure Mode of Test Samples

The typical bond failure modes between steel bars and concrete can be categorized into three main types: steel bar pull-out failure, steel bar yield failure, and concrete splitting failure. The failure modes of the ribbed steel bar-UHPC pull-out samples tested in this study are summarized in Table 3 below.

Table 3 Failure modes of each pull-out sample

No. of sample	Diameter of steel bar /mm	Anchorage length/diameter (l_a/d)	Failure mode
S1	18	4	Pull out the failure
S2	22	4	Pull out the failure
S3	32	4	Splitting failure
S4	18	6	Yield strength of steel bars
S5	18	8	Yield strength of steel bars
S6	22	6	Splitting failure
S7	32	6	Splitting failure
S8	22	6	Splitting failure
S9	32	6	Splitting failure

The typical failure modes of samples under different working conditions are shown in Figure 7 below. Samples S3, S6, and S7 exhibited splitting failure because of insufficient concrete cover thickness, with typical vertical and oblique principal cracks appearing on the sample side surfaces. The anchorage zone experienced splitting failure, as illustrated in Figure 7 a). For samples S1 and S2, the short bond length (4d) and limited bond interface area resulted in insufficient confinement,

 https://doi.org/10.59238/j.pt.2025.03.004

leading to pull-out failure in both samples. The typical failure pattern manifested as radial cracks originating from the loading end on the UHPC surface, accompanied by local bulging and even spalling of the UHPC material, as shown in Figure 7 b).

For samples S4 and S5, owing to their small steel bar diameters, both experienced steel bar yield failure when the anchorage length was large. No obvious cracks were observed on the sample surfaces, as shown in Figure 7 c).

a) Typical splitting failure b) Typical steel bar pull-out failure c) Typical steel bar yield failure

Figure 7 Sample failure mode

The average bond stress–maximum steel bar tensile strain curves for each sample are shown in Figure 8. The green vertical lines in Figure 8 represent the steel bar yield strain reference lines. As shown in the curve in Figure 8 a), when the bond length was small (4d) and the steel bar diameter is large, samples S1, S2, and S3 primarily experienced steel bar pull-out failure and UHPC splitting failure. At this point, the tensile strength of the steel bar was not fully utilized, resulting in relatively low average bond stresses; thus, no steel bar yield failure occurred.

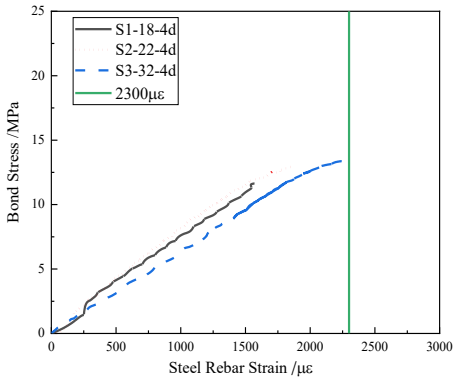

a) Effect of bar diameter on bond stress at an anchorage length of 4d

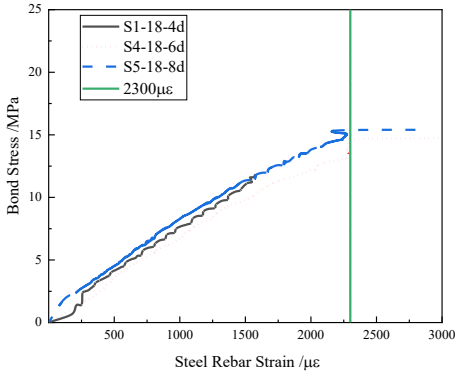

b) Effect of anchorage length on bond stress for 18 mm diameter bars

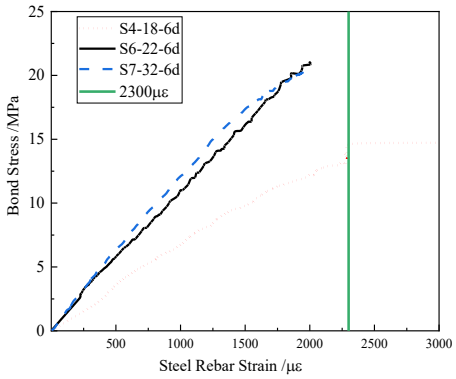

c) Effect of bar diameter on bond stress at an anchorage length of 6d

Figure 8 Curves of average bond stress versus maximum steel strain

When the steel bar diameter remained constant (18 mm), increasing the anchorage length from 4 d to 8 d resulted in a noticeable yield plateau in the average bond stress–maximum tensile strain curve of samples S4 and S5 near failure, as shown in Figure 8 b). Sample S1 (4d), with a shorter anchorage length, did not exhibit steel bar yielding and instead failed due to pull-out. Analysis indicates that when the steel bar diameter is 18 mm, as the anchorage length increases, the failure mode of the samples transitions from pull-out failure to steel bar yield failure. When the protective layer thickness remains constant (3d) and is sufficiently thick, the steel bar anchored in UHPC exhibits a critical anchorage length, with the critical length ranging between 4d and 6d. The average bond stress–maximum strain curves of the bonded segments of samples S6 and S7 were similar. Owing to the relatively large anchorage length (6d) and relatively small protective layer thickness of the samples, both samples experienced splitting failure.

3.2 *Average Bond Stress–Slip Curve (τ—s Curve)*

Research has shown that the bond stress of a test sample is nonuniformly distributed within the bond length range [29]. For the sake of comparative analysis, in this experiment, the average bond stress of the bonded section is used as the object of analysis, and the calculation formula is as follows:

$$\tau = \frac{F}{A_b} = \frac{F}{\pi d l_a} \tag{1}$$

where A_b is the bonded interface area (mm²), τ is the average bond stress (MPa), F is the experimental pull-off load (kN), d is the steel bar diameter (mm), and l_a is the steel bar bond length (mm).

The average bond stress–slip curves for the bonded sections of each pull-out sample are shown in Figure 9.

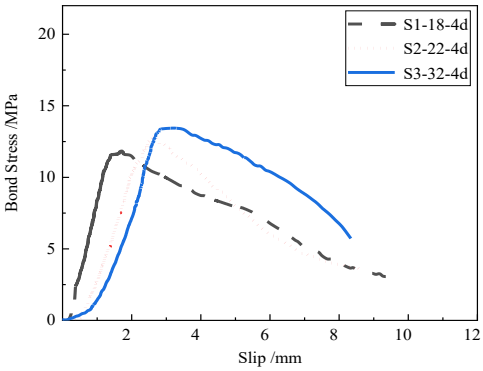

a) Average bond stress–slip curves for S1, S2, and S3

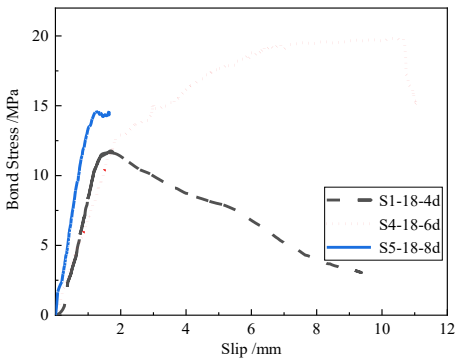

b) Average bond stress–slip curves for S1, S4, and S5

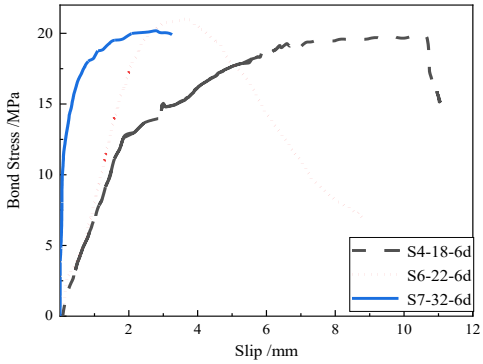

c) Average bond stress–slip curves for S4, S6, and S7

Figure 9 Bond stress–slip curves (τ—s curves) for each sample

https://doi.org/10.59238/j.pt.2025.03.004

According to Chiriatti et al. [30], during the initial loading phase of steel bar extraction, chemical adhesive bonding plays a primary role. Before the maximum bond strength is reached, the average bond stress–slip curves of all the samples exhibit an approximately linear increase in the initial segment. As the load increases, the bond force between the steel bar and UHPC is attributed primarily to mechanical interlocking and friction forces. Owing to the bridging effect of steel fibers, which inhibits crack propagation, the slope of the rising segment of the bond-slip curve between UHPC and ribbed steel bars is greater than that of the bond-slip curve between steel bars and ordinary concrete. When the local tensile stress in the bonded segment exceeds the tensile strength of UHPC, the mechanical interlocking forces gradually weaken, resulting in a significant increase in slip and a corresponding decrease in bond stress. However, compared with the bond stress–slip curve between steel bars and ordinary cement-based materials, the bond stress–slip curve between steel bars and UHPC decreases more gently in the descending segment [29,31]. This characteristic is evident in the bond stress–slip curve with a complete descending segment obtained in this experiment. As shown in Figure 10, a comparison of the ultimate bond stress between steel bars and UHPC in this experiment with the ultimate bond stress between steel bars and ordinary concrete (C40) in the literature [23,29,32] reveals that owing to the dense matrix of UHPC and the bridging effect of steel fibers, the ultimate bond stress between ribbed steel bars and UHPC under the same conditions can be 1.74 times that of ribbed steel bars and ordinary concrete.

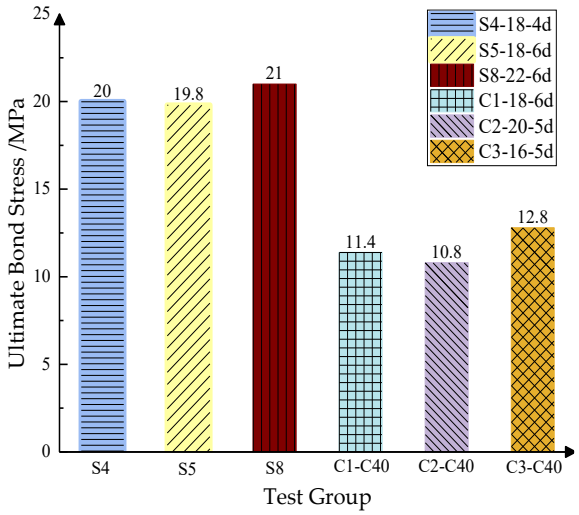

Figure 10 Ultimate bond stress of steel bars in UHPC and ordinary concrete [23,29,30]

3.3 Effect of Steel Bar Diameter and Anchorage Length on Ultimate Bond Stress

When the bond length was 4d for all samples, the bond stress–slip curves of Samples S1 (d = 18 mm), Samples S2 (d = 22 mm), and Samples S3 (d = 32 mm) showed similar trends. The ultimate bond strength of Sample S2 was 10.11% greater than that of Sample S1. Sample S3 (d = 32 mm) failed due to splitting and did not reach the ultimate bond strength; however, its ultimate bond strength was still 3.1% higher than that of S2. When the bond length was 6d, the ultimate bond stress of Sample S4 (d = 18 mm) was 19.03 MPa, and the maximum bond stress of Sample S6 (d = 22 mm) was 21.18 MPa, representing an increase of 11.3% compared with the former. The sample experienced splitting failure. S7 (d = 32 mm) also experienced splitting failure earlier due to insufficient protective layer thickness, with an

ultimate bond stress of 21.08 MPa, and failed to fully utilize the advantage of a larger bond interface area. From the above analysis, it can be concluded that under the same bond length and protective layer thickness and with sufficient protective layer thickness, the bond strength can significantly increase as the steel bar diameter increases. When the anchorage length increased from 4 d to 8 d, the failure mode of samples transitioned from pull-out failure to reinforcement yielding, with the maximum bond stress increasing from 11.82 MPa to 19.85 MPa, representing an increase of approximately 67.94%. Increasing the anchorage length did not affect the bond failure strength of the samples.

4 Adhesion Stress Distribution

The bond stress in the bonded section between the steel bars and concrete is nonuniformly distributed within the bond length [33,34]. The conventional method for determining the bond stress in the bonded section of steel bars involves first directly measuring the strain distribution of the steel bars in the bonded zone, followed by calculating the actual bond stress at the measurement points [35]. Therefore, the bond stress analysis model between steel bars and UHPC can be represented as shown in Figure 11.

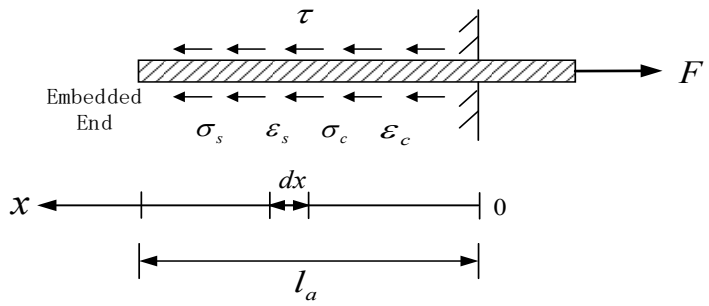

a) Bonded anchoring condition

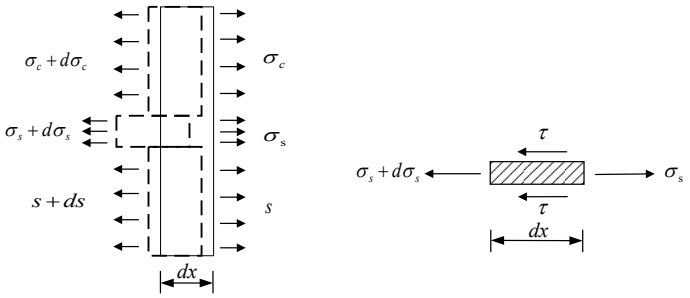

b) Steel bar and UHPC microsegments c) Steel bar microsegments

Figure 11 Bond stress analysis model

By analyzing UHPC microsegments and steel bar microsegments separately, the following formula for calculating the actual bond stress can be obtained:

$$A_s(\sigma_s + d\sigma_s) + \tau \cdot \pi d \cdot dx = A_s\sigma_s \tag{2}$$

$$\tau = -\frac{d}{4} \cdot E_s \cdot \frac{d_\varepsilon}{d_x} \tag{3}$$

where,

τ — bond stress of the micro-segment;

A_s — cross-sectional area of the steel bar in the micro-segment;

 https://doi.org/10.59238/j.pt.2025.03.004

A_c — cross-sectional area of the UHPC in the micro-segment;

σ_s — stress of the steel bar in the micro-segment;

σ_c — stress of the UHPC in the micro-segment;

E_s — elastic modulus of the steel bar, taken as 2.05×10^5 MPa;

E_c — elastic modulus of the UHPC;

ε_s — strain of the steel bar;

ε_c — strain of the UHPC.

In this test, the distance between the strain gauges attached to the pulled-out steel bars was only 1.0d, and the strain measurement points on the steel bars were relatively dense. The bond stress of the steel bars can be calculated using Equation (3). Under different loads, the measured bond stress values of the 18 mm diameter pulled-out samples are distributed along the bond length, as shown in Figure 12, where the x-axis values represent the distance between the strain gauges and the nonloaded end of the sample.

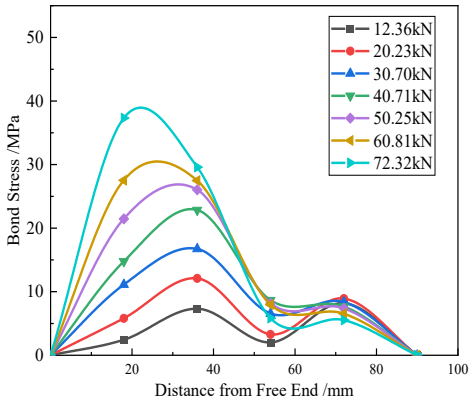

a) Sample S1 (d = 18 mm, l_a = 4d)

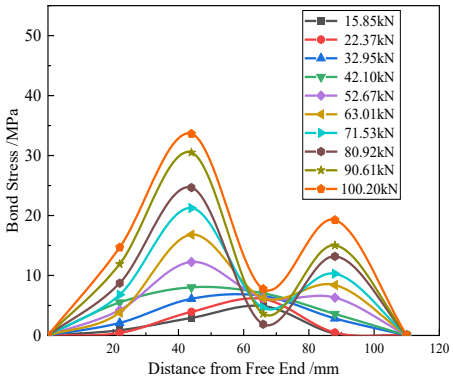

b) Sample S4 (d = 18 mm, l_a = 6d)

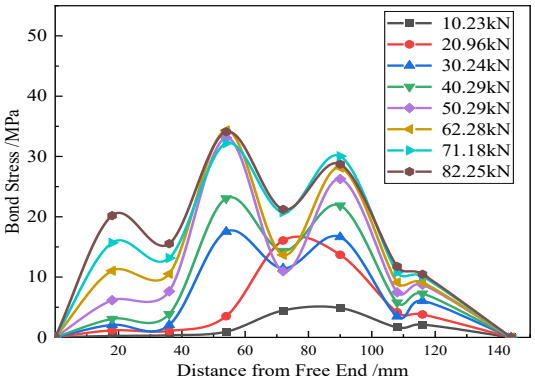

c) Sample S5 (d = 18 mm, l_a = 8d)

Figure 12 Actual measured bond strength–distance curves from the free end

Note: The sampling frequency of the test data is 2 Hz. This graph has been smoothed and fitted using drawing software.

To compare the changes in bond stress distribution during the process of bond strength transition from zero to maximum bond strength, three pull-out samples (S1, S4, and S5) with a steel bar diameter of 18 mm that experienced pull-out failure or steel bar yielding were selected for analysis of the bond stress distribution in the bonded section. The measured bond strength–distance-from-free-end relationship curves for samples S1, S4, and S5 are shown in Figure 12. At low loads (approximately 10 kN), the bond stress distribution was relatively uniform, with the peak bond stress occurring near the loading end. As the load increased, the peak bond stress tended to shift toward the free end, whereas the bond stress

distribution within the bonded section became increasingly nonuniform. The distribution characteristics of the bond stress are related to bond length. As the bond length increased, the bond stress distribution within the bonded section tended to exhibit a multipeak characteristic. When the bond length increased from 4d to 8d, the degree of non-uniformity in the bond stress within the bonded section increased, and the number of bond stress peaks increased from 2 to 3.

Analysis of the test data from this group indicates that for failure modes where the maximum bond stress within the bonded segment can be achieved (either steel bar yielding or pull-out failure), the peak bond stress occurs at approximately $0.4l_a$ from the free end. This finding is consistent with the experimental results reported in Reference [36]. However, the applicability of this conclusion requires further validation with additional test data.

5 Conclusions

Analysis of the bond failure modes, ultimate bond strength, bond stress–slip curves, and steel bar stress distribution characteristics in ribbed steel bar-UHPC pull-out samples reveals the influence of bar diameter and bond length on bond behavior and failure mechanisms. The main conclusions are as follows:

(1) Owing to its dense matrix, high strength, and crack-bridging effect of steel fibers, UHPC demonstrates significantly enhanced ultimate bond strength with steel bars—reaching 1.74 times that of ordinary concrete under comparable conditions. The ascending branch of the bond stress-slip curve exhibits a steeper slope prior to peak stress, while the descending branch shows improved ductility after the ultimate strength is attained.

(2) With sufficient concrete cover thickness, the ultimate bond strength of steel bar-UHPC increases notably with larger bar diameters. Failure modes include bar pull-out or bar yielding. As the anchorage length increases, the failure mode may transition from pull-out to yielding, with bond strength increasing by up to 67.94%. Rational design of the concrete cover thickness can prevent splitting failure in the samples. Under this condition, a critical anchorage length exists for steel bars embedded in UHPC, which falls within the range of 4d and 6d.

(3) For samples experiencing either bar yielding or pull-out failure, the bond stress distribution along the bar embedded in UHPC exhibits a multipeak characteristic. Longer bond lengths lead to an increase in the number of stress peaks and greater non-uniformity in stress distribution. The peak bond stress typically occurs at approximately $0.4l_a$ from the free end. However, the general applicability of this peak stress location requires further validation with additional experimental data.

Conflict of interest: The author disclosed no relevant relationships.

Data availability statement: The data that support the findings of this study are available from the corresponding author, Duan, upon reasonable request.

Funding: This research was funded by Shanghai SASAC Enterprise Innovation Development and Level Improvement Project (grant number is 2024016) and Shanghai Chengtou Group Corporation 2023 Science and Technology Innovation Plan (grant number is CTKY-CYHYD-2023-005). The author extended his sincere gratitude for those supports.

 https://doi.org/10.59238/j.pt.2025.03.004

References

1. Hu,C. Study on the Bending Performance of Ultra-High Performance Concrete Composite Beams. Beijing: Beijing Jiaotong University, 2013.
2. Wang,H. Review of Research on Ultra-high Performance Concrete. China Concrete and Cement Products, 2022, (4): 25-28. doi:10.19761/j.1000-4637.2022.04.025.04.
3. SHI C J,WU Z M,XIAO J F,et al.A review on ultra-high performance concrete: Part I. Raw materials and mixture design.Construction and Building Materials,2015,101(1):741-751.
4. Shi,C.; He,W.; Wu,Z.; et al. Influence of Fibers on Mechanical Properties of UHPC. Bulletin of the Chinese Ceramic Society, 2015, 34(8): 2227-2236.
5. YU R,SPIESZ P,BROUWERS H. J. H.Mix design and properties assessment of ultra-high performance fibre reinforced concrete (UHPC).Cement and Concrete Research,2014,(56):29-39.
6. HALIT Y,MERT Y,YARDMC,et al.Mechanical properties of reactive powder concrete containing high volumes of ground granulated blast furnace slag. Cement and Concrete Composites,2010,32(8):639-648.
7. LIU, G.; ZHANG, X.; ZHAO,Y. Structural design and application of ultra-high performance concrete inamusement platform of Flower Expo. Building Structure,2021,51(S2):959-962.
8. Long,P.; Du,X.; Han,Y.; et al. Analysis of the Flexural Performance of Wet Joints in Precast Assembled UHPC Panels . Building Structures, 2021, 51(S2): 1209-1215.
9. AREL H. Effects of curing type, silica fume fineness, and fiber length on the mechanical properties and impact resistance of UHPFRC.Results in Physics,2016,(6): 664-674.
10. Gao,K. Macro-performance and micro-experimental research on active powder concrete. Beijing: Beijing Jiaotong University, 2010. doi:10.7666/d.y1780339.
11. Liu,X. The Effects of Curing Regimes and Sulfate Erosion on the Properties and Microstructure of Ultra-High Performance Concrete. Wuhan: Wuhan University of Technology, 2016.
12. Ju,Y.; Yu,Y.; Wang,D. Effect of steel fiber content on the strength of RPC under different curing conditions. Concrete and Cement Products, 2015, (4): 42-44. doi:10.3969/j.issn.1000-4637.2015.04.011.
13. Guo,Zh.; Shi,X. Principles and Analysis of Reinforced Concrete. Beijing: Tsinghua University Press, 2006.
14. Wang,R.; Ma,X. Experimental Study on the Bonding and Anchoring of Steel bars and Ultra-High Performance Concrete. Urban Roads, Bridges, and Flood Control, 2018, (09): 204-207. doi:10.16799/j.cnki.csdqyfh.2018.09.056.
15. Han,F.; Liu,J.; Liu,J.; et al. Study on Anchorage Behavior of Steel Bar in Ultra-high Performance Concrete. Materials Reports, 2019, 33(S1): 244-248.
16. Qin,C. Study on the Bonding Performance between High-Strength Steel bars and Active Powder Concrete. Jilin: Northeast Electric Power University, 2018.
17. Yan,J.; Zhang,H.; Wu,B. Beam tests on bond behavior between geopolymer concrete and steel bars. Journal of Building Structures, 2019, 40(12): 178-186. doi:10.14006/j.jzjgxb.2018.0376.
18. Dong,H.; Sun,W.; Cao,W.; et al. Experimental study on bond?slip behavior between steel bars and recycled concrete. Journal of Harbin Institute of Technology, 2017, 49(12):82-90. doi:10.11918/j.issn.036706234.201705005.
19. Li,M. Beam-type experimental study and finite element analysis of the bond performance between coated steel bars and concrete. Yantai: Yantai University, 2018.
20. Wang,D. Experimental Study on the Bonding Performance of Reinforced Concrete. Xi'an: Xi'an University of Architecture and Technology, 2010.
21. Song,W. Study on the Bonding Performance of Glass Aggregate Concrete and Steel bars. Shenyang: Shenyang Jianzhu University, 2016.
22. MAINS R.M. Measurement of the distribution of tensile and bond stresses along reinforcing bars. ACI Journal Proceedings,1951,48(11):225-252.
23. Yan,X.; Shi,Q.; Xu,Zh. Experimental Study on Bond Behavior between Concrete and Deformed Steel Bar with Different Steel Bar. Journal of Hunan University(Natural Sciences), 2020, 47(1): 45-52. doi:10.16339/j.cnki.hdxbzkb.2020.01.006.
24. LI X Y,ZHANG J W,LIU J,et al.Bond Behavior of Spiral Ribbed Ultra-high Strength Steel Rebar Embedded in Plain and Steel Fiber Reinforced High-Strength Concrete.KSCE Journal of Civil Engineering,2019,23(10):4417-4430.
25. SOHAIB A,MUHAMAD R,PILAKOUT K,et al. Bond-slip behavior of steel bars in low-strength concrete. Structures and Buildings, 2016, 169 (7): 524-537.
26. ZUO J,DARWIN D.Bond slip of high relative rib area bars under cyclic loading. ACI Structural Journal, 2000,97(2):331-334.
27. MUHAMMAD A S,AMIR M,JUN X,et al. Development length of high-strength steel rebar in ultra high performance concrete.Journal of Materials in Civil Engineering,2013,25(8):991-998.
28. YUAN J,GRAYBEAL B A.Bond behavior of reinforcing steel in Ultra-high performance concrete. McLean,VA, FHWA, 2014.

29. Mi,Y.; Pan,J.; Zhou,Q. Experimental study on bond behavior between steel bars and patterned vertical alignment engineered cementitious composite. Building Structure, 2016, 46(15): 69-73.
30. CHIRIATTI L,MERCADOM H,APEDO K L,et al.A study of bond between steel rebar and concrete under a friction-based approach.Cement and Concrete Research,2019,(120):132-141.
31. Liu,P.; Li,Y.; Liu,K. Bond performance of HRB500 steel. Journal of Hebei University of Technology, 2012, 41(1): 76-80. doi:10.3969/j.issn.1007-2373.2012.01.017.
32. An,M.; Jia,F.; Yu,Z.; et al. Bond properties of reinforcement anchored in reactive powder concrete flexural members. Journal of Harbin Institute of Technology, 2013, 47(8): 105-110.
33. XING G H,CHENG Z,WU T,et al.Experimental study on bond behavior between plain reinforcing bars and concrete.Advances in Materials Science and Engineering,2015,(6):1-9.
34. SOMAYAJI S.,SHAH S P. Bond stress versus slip relationship and cracking response of tension members. Journal Proceedings,1981,78(3):217-225.
35. DANG C N,MURRAY C D,FLOYD R W,et al.Analysis of bond stress distribution for prestressing strand by Standard Test for Strand Bond. Engineering Structures, 2014,(72):152-159.
36. Jia Fangfang. Experimental Study on the Bonding Performance of Steel bars and Active Powder Concrete. Beijing: Beijing Jiaotong University, 2013.

AUTHOR BIOGRAPHIES

Xinzhi Duan
M.E., Senior Engineer. Graduated from Tongji University in 2012. Working at Shanghai Municipal Planning & Design Institute Co., Ltd.
Research Direction: Development and Application of New Materials and Structures in Civil Engineering.
Email: 496024331@qq.com

 https://doi.org/10.59238/j.pt.2025.03.004